

PACS numbers: 68.37.Hk, 68.37.Lp, 78.67.Qa, 81.16.Pr, 81.20.Wk, 82.33.Pt, 82.65.+r

## Mechanochemical Synthesis of Nanodispersed Compositions on the Base of Zn, Ce and Mo Oxides

O. Sachuk, V. Zazhigalov, S. Shcherbakov, K. Wieczorek-Ciurowa, and I. Bacherikov

*Institute for Sorption and Problems of Endoecology, N.A.S. of Ukraine,  
13, General Naumov Str.,  
UA-03164 Kyiv, Ukraine*

The mechanochemical treatment (MChT) influence on the physicochemical properties (XRD, DTA, SEM, TEM, *etc.*) of molybdenum oxide and binary systems based on zinc, cerium and molybdenum oxides with equimolecular ratio of reagents is studied. The change of phase composition, crystal structure, electronic and catalytic properties of the  $\text{MoO}_3$ ,  $\text{ZnO/CeO}_2$ ,  $\text{ZnO/MoO}_3$  and  $\text{CeO}_2/\text{MoO}_3$  mixtures as a result of mechanical milling is determined. As shown, the mechanochemical treatment of  $\text{ZnO/MoO}_3$  system leads to the formation of nanodimensional  $\text{MoO}_3 \cdot 0.5\text{H}_2\text{O}$  with subsequent formation of  $\text{ZnMoO}_4$  phase with monoclinic modification as nanorods. The formation of nanosize particles of initial oxides and ones of 'core-shell'-type structure with a layer of amorphous molybdenum oxide on a core of nanocrystalline cerium oxide is observed in  $\text{CeO}_2/\text{MoO}_3$  system during the mechanochemical process. As shown, the  $\text{MoO}_3$ -containing systems after the mechanochemical activation of them demonstrate high activity and selectivity to acetaldehyde in process of ethanol oxidation (at  $205^\circ\text{C}$  with a maximum yield of 94–96% for this product). The high photocatalytic activity under visible-light irradiation of the activated Zn–Ce–O samples in organic dye (safranin-T) degradation process in water solution is also observed. Obtained results demonstrate an increase of rate constant from  $0.01 \cdot 10^{-4}$  up to  $3.7 \cdot 10^{-4} \text{ s}^{-1}$  as a result of treatment and show the promising their use in environmental protection processes.

Досліджено вплив механохімічного оброблення (МХО) на фізико-хімічні властивості (РФА, ДТА, СЕМ, ТЕМ тощо) оксиду Молибдену та бінарних систем на основі оксидів Цинку, Церію та Молибдену з еквімолекулярним співвідношенням реагентів. Визначено зміну фазового складу, кристалічної структури, електронних і каталітичних властивостей сумішей  $\text{MoO}_3$ ,  $\text{ZnO/CeO}_2$ ,  $\text{ZnO/MoO}_3$  та  $\text{CeO}_2/\text{MoO}_3$  в результаті механічного подрібнення. Показано, що механохімічне оброблення системи  $\text{ZnO/MoO}_3$  веде до утворення нанорозмірного оксиду Молибдену

$\text{MoO}_3 \cdot 0,5\text{H}_2\text{O}$  з подальшим утворенням фази  $\text{ZnMoO}_4$  моноклінної модифікації у вигляді нанострижнів. В процесі механохімічного оброблення системи  $\text{CeO}_2/\text{MoO}_3$  спостерігалось утворення нанорозмірних частинок вихідних оксидів і частинок типу «ядро-оболонка» з шаром аморфного оксиду Молибдену на ядрі з нанокристалічного оксиду Церію. Показано, що  $\text{MoO}_3$ -вмісні системи після механохімічної активації їх демонструють високу активність і селективність до ацетальдегіду в процесі окиснення етанолу (при  $205^\circ\text{C}$  з максимальним виходом цього продукту у 94–96%). Також спостерігається висока фотокаталітична активність активованих зразків  $\text{Zn-Ce-O}$  за опромінення видимим світлом у процесі деградації органічного барвника (сафраніну Т) у водному розчині. Одержані результати демонструють збільшення константи швидкості від  $0,01 \cdot 10^{-4}$  до  $3,7 \cdot 10^{-4} \text{ c}^{-1}$  в результаті оброблення і свідчать про перспективність використання їх у процесах захисту навколишнього середовища.

**Key words:** mechanochemical treatment, oxide mixture, zinc molybdate, nanorods, ethanol, acetic aldehyde, photocatalyst.

**Ключові слова:** механохімічне оброблення, оксидна суміш, молібдат Цинку, нанострижні, етанол, оцтовий альдегід, фотокаталізатор.

*(Received 1 June, 2021; in revised form, 8 June, 2022)*

## 1. INTRODUCTION

The analysis of the literature data shows that, over the past 25–30 years, the mechanochemical approach to the synthesis of substances, which include nanosize materials, has been successfully applied to various classes of chemical compounds: metals and solid solutions, oxides and complex oxides, inorganic and organic compounds, etc. The processes, which are promoted by mechanochemical treatment of solid substances, were described in detail in Refs. [1–4]. Application of mechanochemistry to the catalysis is one of the interesting but insufficiently studied problem in our opinion, and there are some works devoted to investigations in this area [5, 6]. The analysis of results presented in these works shows that mechanical activation of solid reagents is usually attributed (see the reviews [7–14]) to the significant increase of their surface area and the development of extremely reactive states with crystal-lattice defects, vacancies, free radicals, various structural abnormalities, new surfaces, etc., which lead to the chemical transformations of reagents. An advantage of such a method of activation of the reaction mixture is the absence of solvent (in most cases) and problems concerned with recovery of the reaction products from the solution and the utilization of the solvent. In addition, such processes proceed at significantly lower temperatures (often, they do not require any

heat) than the analogous reactions without mechanical activation of the reagents.

Recently, the method of mechanochemical activation is used more often for synthesis of nanosize compounds including the binary compositions. Interest to two-component oxide systems based on Zn, Ce and Mo oxides is determined by their unique properties, because they are used in modern electronics, adsorption, catalysis, photocatalytic process, *etc.* [15–27]. The analysis of results presented in these publications shows that the use of traditional methods of synthesis leads to the formation of new nanodimensional compounds in oxides' mixtures consisting of Zn, Ce and Mo oxides, which improve greatly their functional characteristics. For example, the formation of metal molybdates, improvement their catalytic properties in these synthesis [22–24, 28–37] was shown too. In relation to mechanochemical activation of some systems containing the ZnO and CeO<sub>2</sub> oxides, an increase of their photocatalytic activity in organic dyes, destruction and formation of nanosize compositions with spinel structure were found [38–46]. Nevertheless, the application of promising mechanochemical method for the ZnO/MoO<sub>3</sub>, CeO<sub>2</sub>/MoO<sub>3</sub> and ZnO/CeO<sub>2</sub> systems' change of solid-state reactivity and synthesis of new compounds were not described.

Our article presents the results of mechanochemical treatment of both MoO<sub>3</sub> and complex oxide systems ZnO/MoO<sub>3</sub>, CeO<sub>2</sub>/MoO<sub>3</sub> and ZnO/CeO<sub>2</sub> with molar ratio of initial oxides 1:1.

## 2. EXPERIMENTAL

Complex oxide systems ZnO/MoO<sub>3</sub>, CeO<sub>2</sub>/MoO<sub>3</sub> and ZnO/CeO<sub>2</sub> with molar ratio of oxides 1:1 were prepared by mixing of corresponding oxides' powders (all reagents were marked 'pure'). Milling was carried out in a planetary ball mill Pulverisette-6 (vial and balls from ZrO<sub>2</sub>) in air atmosphere at rotation frequency of 550 rpm with the reverse after every 30 min of milling. For all experiments, 10 g of the powder was placed in vial (200 cm<sup>3</sup>); ball-to-powder mass ratio (BPR) was equal to 10. Duration of activation was of 2, 4 and 8 hours. The study of structure and physicochemical properties of the synthesized samples was carried out by methods presented below.

Powder x-ray diffraction pattern of the samples was obtained with CuK<sub>α</sub> radiation ( $\lambda = 1.54056 \text{ \AA}$  at 40 kV, 30 mA) using a diffractometer PW 1830 Philips. The sample was scanned over the required range for  $2\Theta$  values (10–90°). The crystallite size ( $L$ ) for the compositions was calculated using Debye–Scherrer formula, according to Eq. (1):

$$L = 0.9\lambda/\beta\cos\Theta, \quad (1)$$

where  $\lambda$  is the x-ray wavelength (for  $\text{CuK}\alpha$ ,  $\lambda \approx 0.154$  nm),  $\beta$  is the line broadening at half-maximum intensity (FWHM) in radians, and  $\Theta$  is the Bragg angle.

The specific surface area was calculated using the BET method and the total pore volume was established from the adsorption-desorption isotherms of nitrogen on 'NOVA-2200', Gas Sorption Analyzer (Quantachrome, United States).

The FT-IR spectra were recorded on a spectrometer 'Spectrum-One' (Perkin-Elmer Instruments) in air atmosphere at room temperature in absorbance mode (mass ratio sample/KBr = 1:20) in the range 4000–400  $\text{cm}^{-1}$ .

EPR spectra were obtained on a Bruker Elexsys E580 FT/C at room temperature at a frequency of 9.2–9.9 GHz.

The surface structure of compositions was determined by transmission electron microscopy method using device JEM 1230 (Jeol) after previous ultrasound dispersing of samples in ethanol.

The adsorption organic dye safranin-T on obtained samples was studied by the method from Ref. [12]. The equilibrium concentration of safranin-T was determined by spectrophotometric method on the UV-2450 Shimadzu instrument. The initial ratio of the solid sample mass to solution volume was 1:4 (12.5 mg:50 ml). The sorption degree ( $S$ ) and adsorption capacity ( $a$ ) were calculated by Eqs. (2) and (3):

$$S = \{(C_0 - C_{\text{eq}})/C_0\} \cdot 100\%, \quad (2)$$

$$a = (C_0 - C_{\text{eq}}) \cdot V/m_s, \quad (3)$$

where  $a$  is adsorption capacity [g/l],  $C_0$  is initial concentration of dye solution [g/l],  $C_{\text{eq}}$ —equilibrium concentration [g/l],  $V$ —solution volume [ml],  $m_s$ —sorbent mass [g].

Catalytic activity of the samples in the ethanol oxidation was tested in a flow fixed-bed stainless microreactor at atmospheric pressure in the temperature range 25–300°C. The catalyst ( $V = 0.5$   $\text{cm}^3$  with fraction of 0.25–0.50 mm) was loaded into a reactor. Gas mixture containing 1 vol.%  $\text{C}_2\text{H}_5\text{OH}$  in air was passed through the reactor at a total flow rate of 20  $\text{cm}^3/\text{min}$ . Initial components and reaction products have been analyzed by on-line gas chromatography, with flame ionization (FID) and thermal conductivity detectors (TCD). The reaction of ethanol partial oxidation to acetaldehyde occurs according to the equation:



The ethanol conversion, selectivity of products and their yield were calculated according to the following formulas:

$$X_{\text{EtOH}} = \{(C_{\text{EtOH}(\text{in})} - C_{\text{EtOH}(\text{out})})/C_{\text{EtOH}(\text{in})}\} \cdot 100\%, \quad (5)$$

$$S = \{C/(C_{\text{EtOH}(\text{in})} - C_{\text{EtOH}(\text{out})})\} \cdot 100\%, \quad (6)$$

$$Y = X_{\text{EtOH}} \cdot S/100, \quad (7)$$

where  $X_{\text{EtOH}}$  is ethanol conversion [%],  $S$  is selectivity of product,  $Y$ —product yield [%],  $C_{\text{EtOH}(\text{in})}$ —initial ethanol molar concentration,  $C_{\text{EtOH}(\text{out})}$ —ethanol molar concentration after reactor,  $C$ —product molar concentration after reactor.

### 3. RESULTS AND DISCUSSION

#### 3.1. Mechanochemistry of Molybdenum Oxide

In relation to modifying the properties of  $\text{MoO}_3$  by mechanochemical processing of it in this section, we presented the results, which show the possibility of  $\text{MoO}_3$  activation at a wide range of the changes of the amount of oxide loaded, the diameter of the balls, the speed of rotation and ball-to-powder mass ratio, and treatment medium. Nevertheless, it is possible to establish a number of general regularities, to which the mechanochemical activation of molybdenum oxide leads. Firstly, it should be noted that, independently of processing conditions, the increase of time treatment leads to increase of specific surface area of the sample (Fig. 1, *a*, *b*).

At the same time, it is necessary to note that the treatment in air (Fig. 1, *a*) makes the possibility to achieve much larger values of the specific surface area (in Ref. [47], it was shown that the exper-

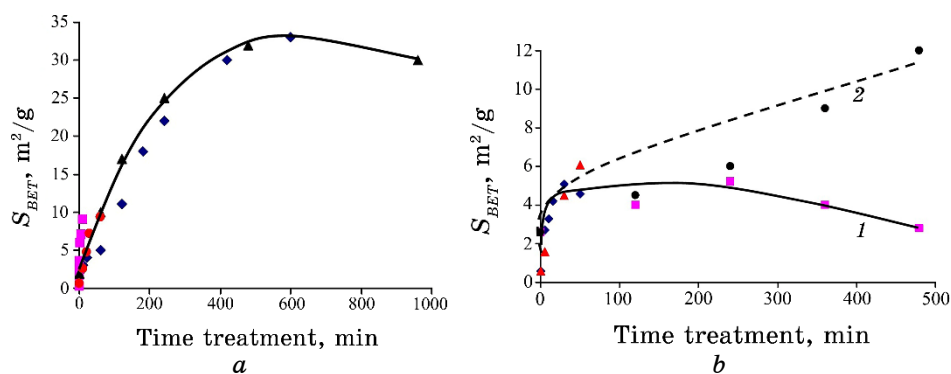


**Fig. 1.** The dependences of the specific surface area of  $\text{MoO}_3$  on the time of treatment: *a*—in air (the results obtained in Refs: [47]— $\blacklozenge$ , [48]— $\bullet$ , [49]— $\blacksquare$ , [50]— $\blacktriangle$ ); *b*—in water (1) and ethanol (2) (the results obtained in Refs: [48]— $\blacklozenge$ , [50]— $\blacksquare$ , [48]— $\blacktriangle$ , [50]— $\bullet$ ).

imental curve of the change in the specific surface area coincides with the calculated one) than the treatment in water and ethanol (Fig. 1, *b*). The results presented in Fig. 1, *b* demonstrate that the treatment in water accompanied by rapid achievement of the specific surface area maximum value, while the maximum is not yet observed in ethanol after 480 minutes of treatment.

In Ref. [48], it was shown that the use of ethanol–water mixture (volume ratio 1:11) as medium leads to a slower increase in the specific surface area compared to the treatment in ethanol but faster than in water. Almost the same behaviour was observed after treatment of  $\text{MoO}_3$  in a benzene–water (1/20 volume ratio) emulsion [48]. In all these studies, it was shown that, simultaneously with an increase in the specific surface area, the particle size of initial oxide decreases up to 32 [49] or 22–24 nm [50, 51] are occurred, and the minimum particle sizes up to 7 nm were observed in Ref. [52]. In addition, it was shown that an increase of processing time (after maximum specific surface area achievement) accompanied by particles' aggregation [49, 50, 52–54] that leads to a decrease of specific surface area of the sample.

The study of  $\text{MoO}_3$  samples after mechanochemical treatment in air permits to establish a decrease of the intensity of all reflections on the diffractograms, their broadening and a change in the relative intensity between reflections [47, 48, 50–52, 54–57], the formation of an amorphous layer on the sample surface [47, 48], and the tran-

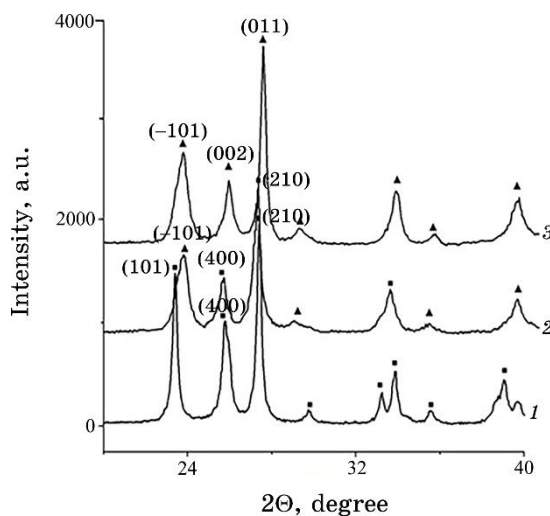


**Fig. 2.** Diffractograms of  $\text{MoO}_3$  after mechanochemical treatment in air at: 200 rpm—1, 400 rpm—2, 600 rpm—3. ■—orthorhombic modification of  $\text{MoO}_3$ ; ▲—monoclinic modification of  $\text{MoO}_3$ . Time treatment is of 4 h in Pulverisette-6; balls and vial of  $\text{Si}_3\text{N}_4$ ; BPR is of 13/1.

sition of the molybdenum-oxide orthorhombic modification to monoclinic [50, 58, 59], with a change in both the number of revolutions (Fig. 2) and the processing time (Fig. 3).

It should be noted that the monoclinic modification of  $\text{MoO}_3$  exhibits higher activity in various catalytic oxidation processes [50, 51, 60–64]. At the same time, as found, this treatment leads to the formation of molybdenum suboxides  $\text{MoO}_{3-x}$  [65] or metastable  $\text{MoO}_{2.8}$ , which can decompose into  $\text{Mo}_{17}\text{O}_{47} + \text{MoO}_3$  [48, 66–69].

Activation in water at high energy loads (3000 rpm, stainless steel equipment) also leads to the formation of molybdenum suboxide  $\Delta\text{-MoO}_{2.8}$  together with the existence of  $\text{MoO}_3$ , and after 50 minutes of treatment, the maximum intensity has a reflex from the plane [021], although, at less time treatment, the maximum intensity was observed on the reflex from the plane [400] [48, 67–69]. Similar effects were observed, when activation of  $\text{MoO}_3$  in the water–ethanol or water–benzene mixtures was realized. Less energy loading (600 rpm,  $\text{Si}_3\text{N}_4$  equipment) leads to an appearance of reflexes of the sidvilit phase ( $\text{MoO}_3(\text{H}_2\text{O})_2$ ) [70] after 4 h of treatment, and with an increase of the time treatment, an amorphization of the oxide proceeds occurs [50, 51].

The mechanochemical treatment of  $\text{MoO}_3$  in ethanol (3000 rpm) [48, 66–69] leads to an increase in the intensity of the reflex from

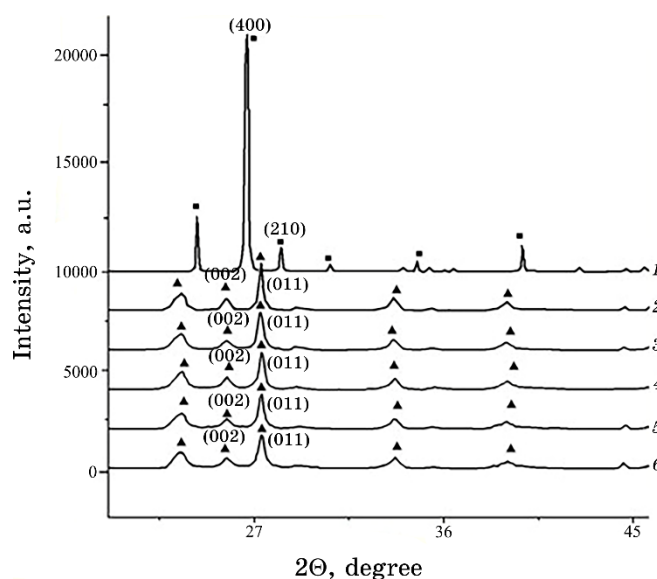


Fig. 3. Diffractograms of  $\text{MoO}_3$ : initial—1; after treatment in air for: 1 h—2, 2 h—3, 4 h—4, 8 h—5, 16 h—6. ■—orthorhombic modification of  $\text{MoO}_3$ ; ▲—monoclinic modification of  $\text{MoO}_3$ . Rate—600 rpm.

the plane [021] with  $d = 0.33$  nm. At the same time, it should be noted that, after 5 minutes of treatment, there is also a sharp increase in the relative intensity of the reflex corresponding to the plane [060]. This intensity increases from 59% for the initial sample to 99%. With an increase of the time processing, the relative intensity of this reflex decreases against to initial value. In the diffractograms of the sample after 50 min of treatment in ethanol, a number of new weak reflexes appear with  $d = 0.58, 0.46, 0.43, 0.41, 0.28, 0.22$  nm, which can be attributed to the non-stoichiometric Magnéli  $\chi$ - $\text{Mo}_8\text{O}_{23}$  phase formed from  $\text{MoO}_3$  by the crystallographic shift mechanism. With a less number of rotations (600 rpm), the delayed transition of the orthorhombic modification to monoclinic  $\text{MoO}_3$  with the subsequent reflexes' appearance of  $\text{Mo}_8\text{O}_{23}$  was observed in comparison to treatment in air [50, 51].

It should be noted that the formation of molybdenum suboxides after treatment of  $\text{MoO}_3$  leads to a sharp increase of the activity of the sample in the reactions of oxidation of *n*-butane and propane [48], ethanol [50], and the possibility of new directions in ethanol oxidation appears [50, 51]. On this sample, the reaction of benzene direct oxidation to phenol by oxygen gas phase was also observed [48, 66–69].

The study of the obtained samples in ethanol oxidation reaction by gas chromatography showed that the initial molybdenum oxide (orthorhombic modification) is a low-active catalyst: the degree of ethanol conversion equal to 50% is reached at 250°C, and the carbon oxides are main products (selectivity of their formation was about 90%). Mechanochemical treatment allows to increase its activity in this process and to change the direction of the ethanol oxidation process (Table 1).

**TABLE 1.** The influence of the  $\text{MoO}_3$  morphology on the properties in ethanol oxidation process.

Medium of MChT	Modifications of $\text{MoO}_3$ , crystal orientation*		Catalytic properties**		
	After MChT	After catalysis	$T_r$ , °C	Selectivity, mol. %	
				$\text{CH}_3\text{CHO}$	$\text{C}_2\text{H}_4$
initial	O-, LP	O-, LP	250	11	0
air	M-, LP	M-, LP	185	97	1
water	Sidvilite	O-, BP	225	10	85
ethanol	O-, BP + M-, LPO-, BP + M-, LP		195	30	68

Note: \*O—orthorhombic; M—monoclinic; LP—lateral plane; BP—basal plane;  
\*\* parameters at a 50% ethanol conversion;  $T_r$ —reaction temperature.

Depending on the medium treatment, crystal modifications of  $\text{MoO}_3$  with different preferential crystallographic orientation are formed. These compounds allow to carry out ethanol oxidation process with a high selectivity for the specific product—acetaldehyde or ethylene [71]. The presence of a monoclinic modification of  $\text{MoO}_3$ , which is formed quite quickly after treatment in air (60 min), with a preferential orientation along the lateral plane allows to form  $\text{CH}_3\text{CHO}$  (Table 1), the selectivity for which decreases at full conversion of ethanol. In the presence of an orthorhombic modification of  $\text{MoO}_3$  with a predominant orientation along the basal plane, which formed from sidvilitite ( $\text{MoO}_3(\text{H}_2\text{O})_2$ ), the high selectivity to ethylene is observed; it only slightly decreases with an increase of conversion up to 100%. The formation of the mixture of two modifications of  $\text{MoO}_3$  (treatment in ethanol) leads to the preparation of catalyst, at which these two products are formed with high selectivity (Table 1).

It can be concluded that mechanochemical activation of  $\text{MoO}_3$  in all mediums leads to an increase of catalytic activity of the sample in ethanol oxidation that can be related with an increase in specific surface area and particles' sizes decrease. The high selectivity for different products can be related with different samples' crystallographic morphology and their influence on the mechanism of substrate activation.

### 3.2. Mechanochemical Activation of ZnO/ $\text{MoO}_3$ System

Practically all industrial catalysts contain in their composition metal oxides as base active phase of the catalysts or the additives to the base catalytic matrix. Many investigations proved the influence of method of oxide catalyst preparation on its dispersion and catalytic activity [72]. In our article, we will show the effect of mechanochemical treatment conditions on the physicochemical and catalytic properties of complex binary oxide systems based on Zn, Ce and Mo.

The results of mechanochemical treatment of the ZnO and  $\text{MoO}_3$  mixtures with different molar ratio of oxides were reported in our publications [73–75]. It was found [74, 75] that mechanochemical treatment of the mixture with equimolar ratio of initial oxides in air permits to obtain nanosize  $\beta\text{-ZnMoO}_4$  monoclinic modification. Traditionally, this phase was prepared from salts of these metals and the different medium use [18]. In this case, the activation of oxides' mixture was carried out in the planetary ball milling Pulverisette-6 in air atmosphere during 2, 4 and 8 hours with balls' ( $\text{ZrO}_2$ ) diameter of 5 mm and BPR 10:1 at rotation frequency of 550 rpm. It was established that, after treatment during 2 h, the intensity of all reflexes for the initial oxides significantly decreases with

**TABLE 2.** Properties of the ZnO–MoO<sub>3</sub> = 1:1 samples after mechanochemical treatment in air.

Time of processing, h	Phase	<i>L</i> , nm	<i>S</i> , m <sup>2</sup> /g	<i>V<sub>s</sub></i> , cm <sup>3</sup> /g	Results of ethanol oxidation			
					<i>X</i> = 50%		<i>X</i> = 100%	
					<i>T<sub>r</sub></i> , °C	<i>S<sub>Ac</sub></i> , %	<i>T<sub>r</sub></i> , °C	<i>S<sub>Ac</sub></i> , %
0	<b>-MoO<sub>3</sub></b> , ZnO	56	2	0.026	260	80	317	61
2	<b>MoO<sub>3</sub>·0.5H<sub>2</sub>O</b> , α-MoO <sub>3</sub> , ZnO	13	5	0.022	211	97	258	91
4	<b>-ZnMoO<sub>4</sub></b> , ZnO, MoO <sub>3</sub> ·0.5H <sub>2</sub> O	18	6	0.027	188	98	215	95
8	β-ZnMoO <sub>4</sub>	15	9	0.037	177	100	205	96

*Note:* The phase with maximum reflexes' intensity on the diffractograms is highlighted bold (in the column of phase); *L*—average crystallite size determined from the maximum intensive reflex; *S*—specific surface area (BET) of the sample; *V<sub>s</sub>*—total pore volume; *T<sub>r</sub>*—reaction temperature; *S<sub>Ac</sub>*—selectivity of acetic aldehyde; *X*—ethanol conversion.

simultaneous reflexes' broadening that can be explained by a decrease of the oxides' particles' size. The data presented in Table 2 and Figures 4, *b*, 5, *b* confirm this fact. In the same time, the appearance of new reflexes related with MoO<sub>3</sub>·0.5H<sub>2</sub>O-phase formation was observed (Table 2).

It can be assumed that the formation of MoO<sub>3</sub>·0.5H<sub>2</sub>O phase occurs due to the presence of water molecules absorbed by initial oxides. The presence of adsorbed water is confirmed by DTA–TG and FT-IR data. The results obtained by DTA–TG demonstrate the sharp mass lose (about 5%) and the shift of endothermic-effect temperature from 260°C (initial oxides' mixture) up to 226°C, which is related with lower temperature of water removal than in initial sample. FT-IR-spectra demonstrate the presence of the characteristic bands of water molecules (1620 and 3560 cm<sup>-1</sup>) for initial mixture and after treatment, and also the shift of the Mo=O, Mo–O–Mo and Zn–O bands (treated sample in comparison to initial mixture) from 991, 864 and 495 cm<sup>-1</sup> up to 982, 857 and 473 cm<sup>-1</sup>, respectively, and the appearance of new band at 955 cm<sup>-1</sup> characteristic for MoO<sub>3</sub>·0.5H<sub>2</sub>O.

The data obtained by SEM (Fig. 4) and TEM (Fig. 5) show the changes of crystallites' size after mechanochemical activation of the mixture. The results presented in Fig. 4, *a*, *b* demonstrate that, in mechanochemical process with sample during 2 h, the destruction of initial crystallites with decrease of their sizes takes place; herewith, it should be noted that larger particles are agglomerates of smaller

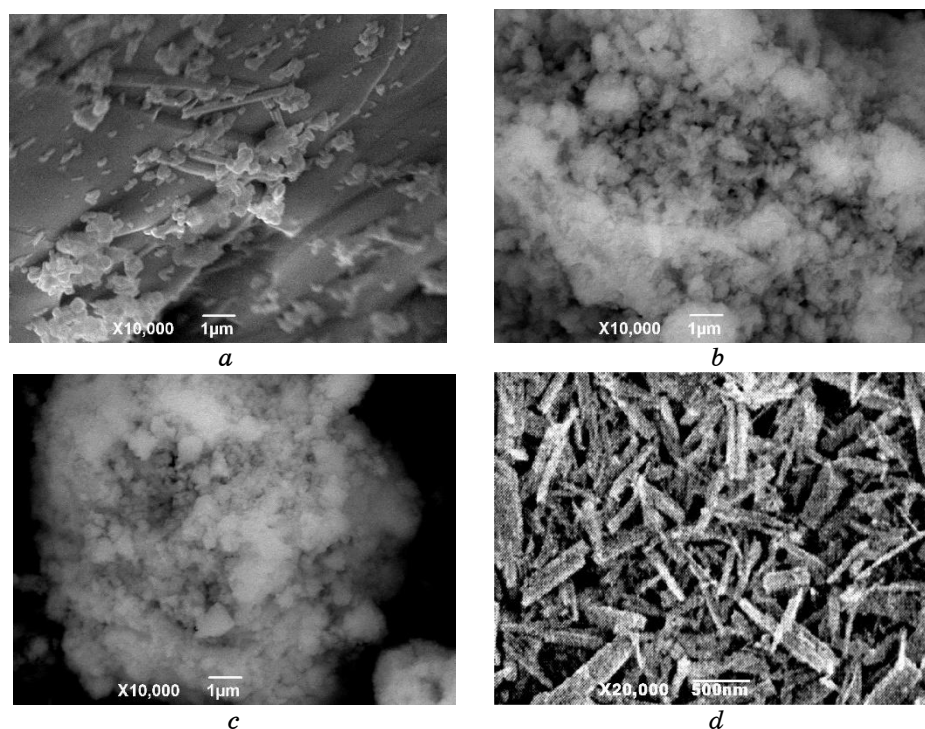
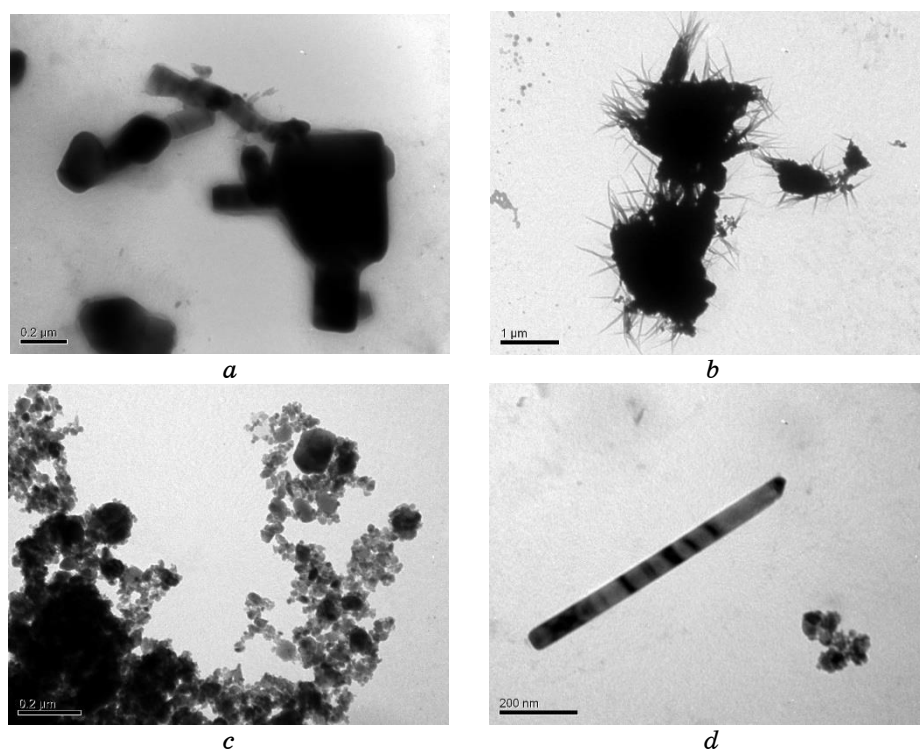


Fig. 4. SEM microphotographs of ZnO/MoO<sub>3</sub> system: initial one—*a* and after MChT during: 2 h—*b*, 4 h—*c*, 8 h—*d*.

crystallites.

Figure 5, *b* shows that, simultaneously with the activation and decrease of particle size, the formation of the particles with new habitus, namely, elongated needles, which can belong to formed MoO<sub>3</sub>·0.5H<sub>2</sub>O phase, occurs (that can be evidenced by data presented in [50, 51] and their disappearance with increase of treatment time). Simultaneously, the presence of rounded crystals, which can be identified as MoO<sub>3</sub>, and small particles as ZnO was observed.

The increase of time of processing up to 4 h, according to XRD data, leads to formation of zinc molybdate β-ZnMoO<sub>4</sub> of monoclinic modification (Table 2). The formation of this phase can be related with two factors: i) high reactivity of the small ZnO particles that was reported in [76, 77], where the mechanochemical treatment of zinc oxide was studied; ii) the presence of hydrated molybdenum oxide, which, according to scheme proposed in Ref. [18], participates in the formation of zinc molybdate phase by means of its traditional synthesis in solution. The study of the sample by SEM method (Fig. 4, *c*) shows the significant decrease of particles' size



**Fig. 5.** TEM microphotographs of ZnO/MoO<sub>3</sub> system: initial one—*a* and after MChT during: 2 h—*b*, 4 h—*c*, 8 h—*d*.

due to the crystal destruction and formation of agglomerates, which contain small particles. TEM data (Fig. 5, *c*) show the disappearance of needle-like particles and an appearance of the number of new rounded light small crystallites, which can be attributed to ZnMoO<sub>4</sub>. The formation of zinc molybdate phase is confirmed by FT-IR data, which demonstrate not only the shift and intensity decrease of the Mo=O, Mo-OH and Zn-O bands (the shoulders at 980, 950 and 470 cm<sup>-1</sup>, respectively, are observed only), but an increase of intensity of metal molybdates bands (for Mo-O-Mo and O-Mo-O at 850 and 652 cm<sup>-1</sup>, respectively). In turn, DTA curve shows the appearance of exothermal effect at 430°C, which can be related with the crystallization of partially amorphous ZnMoO<sub>4</sub> particles, and the shift of endothermic effect, which is related with nano-MoO<sub>3</sub> melting up to 670°C (both without mass loss).

After mechanochemical treatment of the mixture during 8 h only, the reflexes of β-ZnMoO<sub>4</sub> phase with maximum intensity at [-111] are observed by XRD. The study of this sample by SEM method (Fig. 4, *d*) shows the presence of a significant number of

rod-like crystals, while TEM data demonstrate the formation of elongated crystals with cross section equal to 15–35 nm and the length near 100–800 nm. It can be assumed that, in process of mechanochemical activation, the existence of local warming [78] and increased pressure provokes the condensation of small crystals of  $\text{ZnMoO}_4$  in one of the directions of the crystallographic axes with formation of a larger particle carried out. The data presented in Fig. 5, *d* show that, after mechanochemical activation of the mixture during this time, the process of the rod-like  $\beta\text{-ZnMoO}_4$  nanocrystals' formation does not end completely. This is evidenced by presence of small rounded particles of this phase with dimension of 15–25 nm (see Fig. 5, *b*), the formation of which was fixed early (Fig. 5, *c*). It is necessary to note that the formation of  $\beta\text{-ZnMoO}_4$  crystals with similar habitus, namely, nanorods of zinc molybdate was observed in the electrochemical synthesis with use of the monocrystalline molybdenum as reagent [79] only.

According to FT-IR data, all vibrations' characteristics of zinc molybdate are recorded in spectrum of this sample. The absorption bands at 647, 850 and 950  $\text{cm}^{-1}$ , which are corresponding to bending, asymmetric and symmetric stretching vibrations of octahedral  $[\text{MoO}_6]$ -coordinated molybdenum in different metal molybdates [80, 81], are present in spectrum. In addition to the endothermic effects at 124 and 202°C associated with the removal of water, in the DTA curve, the small exothermal effect at 430°C (without any mass loss) is present, and it can be related with crystallization of partially amorphous  $\text{ZnMoO}_4$  rounded particles (Fig. 5, *d*), while the effect at 670°C, which responds to melting of nanocrystals of  $\text{MoO}_3$ , is absent. All obtained results demonstrate that, in mechanochemical processing (after 8 h treatment), formation of zinc molybdate is finished practically, but there is not its crystallization (or nanorods' condensation), and part of this composition is in amorphous state.

Simultaneously, it is necessary to note that the mechanochemical activation of the samples leads to an increase of specific surface area and pore volume (Table 2). It should be noted that, in mechanochemical process with the Zn/Mo mixture, the change of the value of specific surface area is significantly smaller than under treatment of individual  $\text{MoO}_3$ , where the specific surface area is increased up to 33–35  $\text{m}^2/\text{g}$  [51, 77, 82]. This difference in specific surface area can be explained by fact that, in the mechanochemical process of the mixture, not only the grinding of  $\text{MoO}_3$  is carried out but the chemical reaction with formation of new compositions, for example, zinc molybdate occurs too.

Taking into account that molybdenum oxide after mechanochemical activation in air showed the promising properties in reaction of ethanol oxidation to acetaldehyde (Table 1 and [51]), the catalytic

activity of the Zn–Mo–O samples prepared in this reaction was studied. The results presented in Table 2 demonstrate an increased catalytic activity (ethanol conversion degree) and reduction of the reaction temperature for the samples after treatment. This fact can be associated with an increase of specific surface of the samples as a result of treatment. In addition, a significant change in the selectivity of acetaldehyde formation was also observed.

On the other hand, the comparison of specific rates of ethanol oxidation shows (Fig. 6) the presence of two regions in its dependence on the specific surface area. First region (low reaction rate) can be related with an increase of specific surface area and practically correspond to G. Boreskov's rule [83], which determines the stability of specific rate of oxidation at different sample-preparation methods. However, the formation of zinc molybdate leads to abrupt increase of specific rate of ethanol oxidation (second part with high value of the rate). So, two different compounds can determine the specific rate of ethanol oxidation of the Zn–Mo–O mixture: in first case, this is molybdenum oxide (it is necessary to note that this value is near to obtained one for treated  $\text{MoO}_3$ ) and, in second case, the properties of the sample are determined by the presence of zinc molybdate phase, and its crystallization (after 8 h treatment) increases activity. Therefore, zinc molybdate phase can be an active component of the catalyst selective ethanol conversion to acetaldehyde. On the other hand, this phase prepared by traditional method shows a decrease the selectivity at an increase of ethanol conversion (from 90% at 50% conversion up to 75% at 100% conversion) unlike the samples obtained by mechanochemical route (Table 2). Thus, we can conclude that high selectivity for acetaldehyde in the ethanol-oxidation reaction related with the existence in the catalyst nanosize zinc molybdate phase in nanorods form. Low reaction temperature in the presence of the synthesized catalyst at

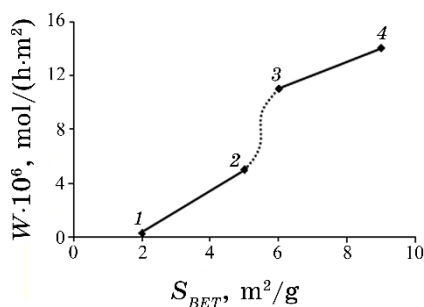


Fig. 6. Dependence of specific ethanol-oxidation rate on the specific surface area (BET) of the initial samples (1) in Zn/Mo system and after MChT of it during: 2 h—2, 4 h—3, 8 h—4.

high product yield (96%) and its productivity (1.8 mol/(kg·h)) shows that the process of ethanol direct oxidation by air on this catalyst can be a promising alternative to known Wacker process, in which acetaldehyde is produced by hydration of ethylene in the presence of complex  $\text{PdCl}_2 + \text{CuCl}_2$  catalyst.

### 3.3. Mechanochemical Treatment of $\text{CeO}_2/\text{MoO}_3$ System

This work fills up the lack of systematic studies on the mechanochemical synthesis and modification of Ce–Mo–O compositions. This section presents the results of the study of MChT effect of an oxide mixture based on cerium and molybdenum (Ce/Mo=1:1) on their physical and chemical properties.

The mechanochemical milling of oxides' mixture  $\text{CeO}_2/\text{MoO}_3=1:1$  (similarly to Zn/Mo system) in air leads to sharp decrease of particle size of oxides (the results of particles' sizes calculations are presented in Table 3). It should be noted that, after MChT (independent on the time of treatment), the change of dominant reflexes (from  $\text{MoO}_3$  to  $\text{CeO}_2$  with maximum reflex from the plane [111]) occurs, herewith the  $\text{MoO}_3$  phase becomes as x-ray amorphous.

This fact is confirmed by SEM (Fig. 7, *a, b*) and TEM (Fig. 8, *b–d*) data. Comparison of the SEM and EDS analyses (Fig. 7, Table 4) shows that big particles (habitus of 200–300 nm—**A**) in initial sample belong to  $\text{MoO}_3$ , while small particles with sizes of 50–70 nm (**B**) are characteristic to cerium oxide. After MChT during 2 h, in the sample, there are large particles (**A**), but their morphology differs from  $\text{MoO}_3$  (looser).

Simultaneously, the results of analysis of these particles (Table 4) show for them the equivalent content of molybdenum and cerium, as in other places on the surface (**B–E**), where presence of fine particles is observed. In addition, it should be noted that, in most of the studied places of surface, there is a slightly lower content of Ce than Mo (Table 4) that can indicate a partial coating of the surface of cerium oxide by molybdena. This assumption is in agreement with data presented in Table 3, which demonstrate the decrease of particle size.

This fact is also confirmed by TEM method (Fig. 8). From Figure 8, *b*, it can be seen the partial amorphization of molybdenum oxide (light particles) and formation the needle-like crystals that characterizes the formation of hydrated molybdenum oxide  $\text{MoO}_3 \cdot 0.5\text{H}_2\text{O}$  (see above). The formation of needle-like crystals with a significant advantage of their length over the cross section leads to the fact that, during following processing, they quickly crush (shorten), and the next coating process of small particles of molybdenum oxide on the larger  $\text{CeO}_2$  crystals takes place.

**TABLE 3.** Some properties of  $\text{CeO}_2/\text{MoO}_3 = 1:1$  composition.

Time of treatment, h	$L, \text{nm}^*$		$S_{\text{BET}}, \text{m}^2/\text{g}$	$V_s, \text{cm}^3/\text{g}$	Selectivity of Ac	
	$\text{MoO}_3 [020]$	$\text{CeO}_2 [111]$			at $X = 50\%$ at $X = 100\%$	
0	93	53	2	0.03	82	61
2	7	21	5	0.06	98	92
4	—	18	3	0.03	100	97
8	—	15	3	0.03	100	96

*Note:* Average crystallite size calculated for most intensive reflexes;  $X$ —ethanol conversion.

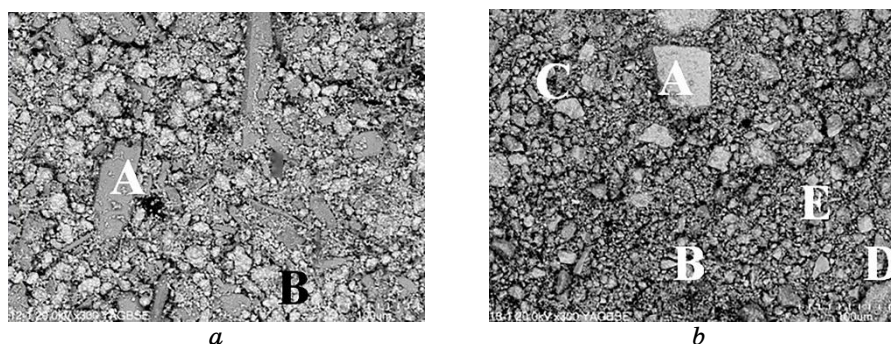


**Fig. 7.** SEM images of initial composition  $\text{Ce}/\text{Mo} = 1:1$  (a) and after 2 h of MChT of it (b).

It should be noted that a similar deposition process during mechanochemical treatment was established for the  $\text{V}_2\text{O}_5/\text{TiO}_2$  system [84], and for the  $\text{MoO}_3/\text{TiO}_2$  system, it is at hydrothermal synthesis [85].

The increase of time of treatment up to 4 h is accompanied by formation of the composites with core-shell structure (Fig. 8, c), whose the beginning can be observed already after 2 h of activation (see Fig. 8, b, b1).

The particles of crystalline  $\text{CeO}_2$  (25–35 nm) play role of core in these composites, and amorphous  $\text{MoO}_3$  is a transparent shell (5–10 nm). It is necessary to note that formation of these core-shell structures was clearly observed at longer time of mechanochemical treatment [86]. The partial formation of core-shell structure already at 2 h treatment well agrees with EDS data, which show the uniform distribution of Mo and Ce in different points of the sample surface (Table 4).

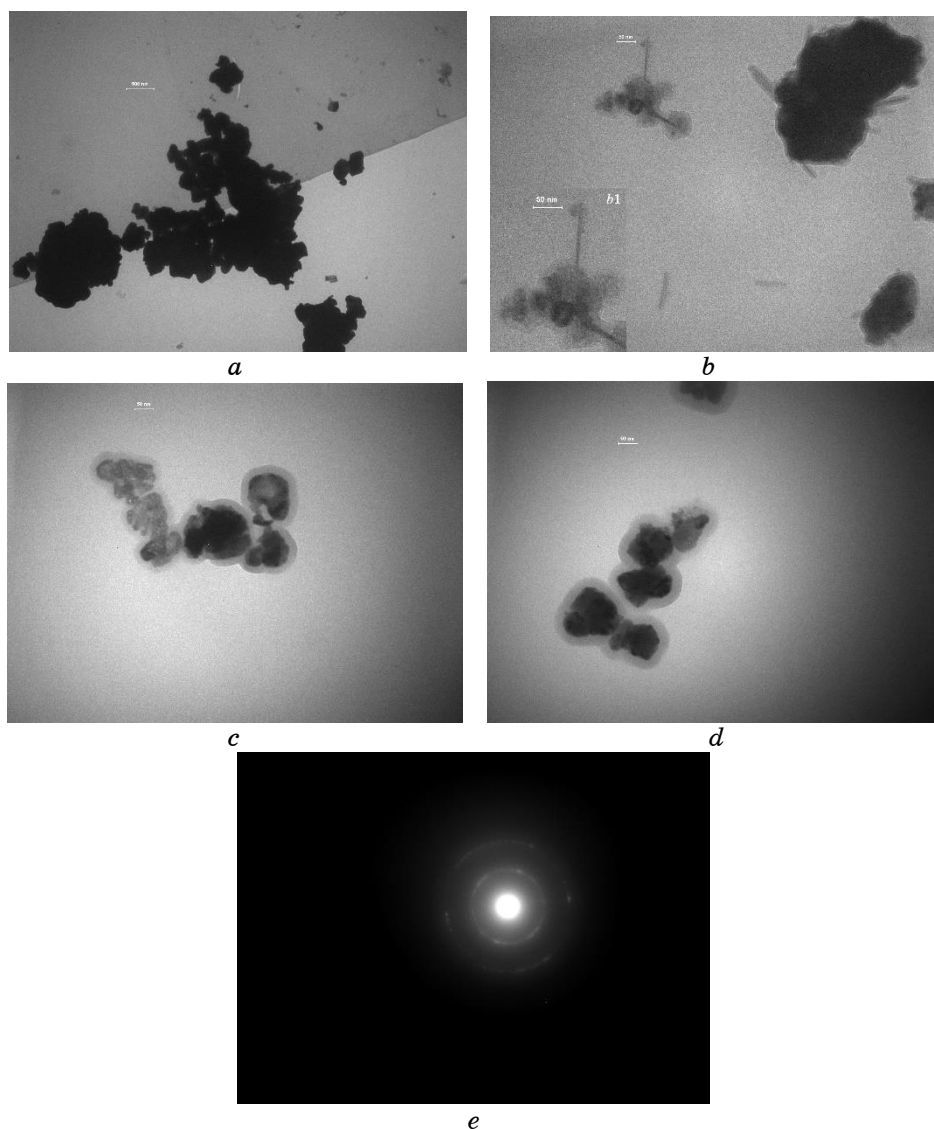


**Fig. 8.** TEM microphotographs of  $\text{CeO}_2/\text{MoO}_3$  samples after MChT during: 2 h—*b*, 4 h—*c*, 8 h—*d*; electron graphic study—*e*; initial sample—*a*.

Longer treatment time (8 h) leads to that the sample contains only the particles of core-shell structure, and their number increases (Fig. 8, *d*). Simultaneously, it can be seen that core is a conglomerate of the particles with dimensions near 10–15 nm, a shell thickness increases up to 10–15 nm. The increase of shell thickness can be related with disappearance of round transparent particles (amor-

**TABLE 4.** EDS analysis of CeO<sub>2</sub>-MoO<sub>3</sub> system.

Element	Initial			After 2 h MChT					
	A	B	FS*	A	B	C	D	E	FS*
Mo	96.5	0	50.2	51.3	51.8	52.2	50.1	46.5	50.5
Ce	3.5	100	49.8	48.7	48.2	47.8	49.9	53.5	49.5

Note: FS—full surface.

phous molybdenum oxide); their presence can be observed in Fig. 8, *c*. The presence of crystalline CeO<sub>2</sub> only in the sample was confirmed by electron graphic investigations (Fig. 8, *e*).

According to FT-IR data except the shifting of absorption band of Mo=O bond from 935 (initial mixture) to 952 (2 h MChT) and 980 cm<sup>-1</sup> (4 h MChT) in spectra of treated samples, the disappearance of absorption band of  $\nu_{as}$  O-Mo-O bond at 622 cm<sup>-1</sup> after 2 h treatment occurs due to MoO<sub>3</sub> amorphization. As to absorption bands of  $\nu_{as}$  Mo-O-Mo and  $\nu_s$  Mo-O, the initially shifts from 825 to 836 cm<sup>-1</sup> and from 801 to 797 cm<sup>-1</sup>, respectively, were established, but, after 4 h activation, they disappear in spectre. Such changes in IR-spectra are in good agreement with the data obtained by XRD, TEM and DTA-TG methods. The last showed the presence of the exothermic effect at 405°C without mass loss that is related with crystallization process of amorphous molybdena (after 4 h of treatment of the sample). Thus, all the obtained results permit to suggest the following mechanism of transformations in the CeO<sub>2</sub>/MoO<sub>3</sub> system as a result of mechanochemical treatment. The action of mechanical energy under treatment provokes the chaotic destruction of CeO<sub>2</sub> crystals and the decrease of their size (Table 3). At the same time, anisotropic destruction of MoO<sub>3</sub> crystals by the crystallographic shear mechanism, noted as early as [57], occurs and leads partially to hydration of molybdenum oxide and the formation of its needle-like crystals, as well as the formation of structural defects and partial amorphization of the molybdenum oxide. The formation of structural defects associated with the appearance of unsaturated Mo<sup>5+</sup> ions ( $g_{\perp} = 1.941$  and  $g_{\perp} = 1.956$  correspond to hexa-co-ordinated Mo<sup>5+</sup> ions in MoO<sub>3</sub> crystal) and transition of the Mo<sup>5+</sup> ion from tetra- to pentagonal co-ordination, which was established by the ESR method. ESR spectra of Ce<sup>3+</sup> ( $g = 1.960$ ) were not recorded for samples after activation.

The study of catalytic properties of Ce/Mo system in ethanol-oxidation process shows the high selectivity of acetaldehyde formation (like to Zn/Mo system). So, at alcohol conversion of 50%, the selectivity to acetaldehyde is of (or close to) 100% (Table 3). The increase of catalytic activity of treated samples can be ex-

plained by decrease of particle size (Table 3) as a result of treatment and corresponding increase of their specific surface area, *i.e.*, number of catalytically active centres. In addition, the increase of catalytic activity of the samples after MChT can be caused by the presence of tetrahedral-co-ordinated  $\text{Mo}^{5+}$  ions, which can easily co-ordinate oxygen with formation of  $\text{Mo}^{6+}\text{-O}_2^-$  couples, and oxygen ions can activate the process oxidation.

It should be noted that the increase of ethanol conversion accompanied by a decrease of the selectivity of acetaldehyde formation, but it remains high even at full ethanol conversion. The maximal yield of this product (97%) can be obtained in the sample after 4 h treatment. However, the temperature to achieve this value is by  $20^\circ\text{C}$  above than in the case of the sample after 8 h treatment, where the yield is equal to 96% (at  $195^\circ\text{C}$ ). A comparison of the obtained results with the literature data related with acetaldehyde production from ethanol shows that they are better than in the best known catalyst  $\text{Ag}/\text{Si}_3\text{N}_4$  [83], where similar results (yield 95%) were obtained at  $300^\circ\text{C}$ .

Therefore, the obtained results show the perspective of creation of new process of acetaldehyde production on the base of renewable raw material—bioethanol as alternative of Wacker process.

The calculation of specific rate of ethanol oxidation shows (Fig. 9) the sharp increase of its value for the samples after treatment in comparison with initial mixture of oxides and practically equal value for the treated samples. In the last case, the Boreskov's rule, which determines the rate constancy for the samples, the same composition, independently on their preparation methods, is fair. This fact permits to conclude that active component of the catalysts

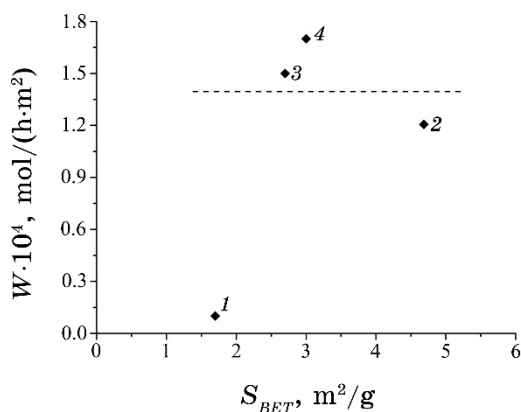


Fig. 9. Dependences of specific ethanol-oxidation rate on the specific surface area (BET) in initial samples 1 and after MChT during 2 h—2, 4 h—3, 8 h—4.

is the composite with core-shell structure, which can be obtained very easily by mechanochemical treatment of initial oxides' mixture in air without solvents and/or metal salts' using.

### 3.4. Mechanochemical Activation of ZnO/CeO<sub>2</sub> System

After considering the data related with mechanochemical treatment of the ZnO/MoO<sub>3</sub> and CeO<sub>2</sub>/MoO<sub>3</sub> compositions, this is a logical extension to study the ZnO/CeO<sub>2</sub> system. The results of mechanochemical treatment influence on the properties of ZnO/CeO<sub>2</sub> composition with molar ratio of the oxides 1:1 will be presented below. It was found that, in mechanochemical activation process, the essential decrease of oxides' particles' size from 174 up to 40 nm for ZnO and from 57 up to 20 nm for CeO<sub>2</sub>, and formation of Zn-Ce-O nanocomposite as a result of treatment is occurred.

The increase of specific surface area of the sample after treatment by up to three times was established (Table 5) too. The destruction of mesopores, which was recorded by us after 2 and 4 h of MChT and partial particles' aggregation with formation of the composite with macroporous structure at an increase of time of treatment, was observed. This fact was confirmed by TEM data (Fig. 10).

It is necessary to note that formation of Zn-Ce-O nanocomposite with similar heterostructures, where the small CeO<sub>2</sub> particles were distributed on the surface of ZnO nanoparticles (Fig. 10, *d*), at its preparation by other methods was shown early [87].

The study of the catalytic properties of MChT-prepared samples in ethanol-oxidation reaction shows their low activity and selectivity to acetaldehyde formation in this process. Therefore, it is possible to conclude that high effectiveness of the catalysts in this process is related with the presence of molybdenum ions in the catalyst in the form of amorphous layer in core-shell composite or in nanoparticles (nanorods) of zinc molybdate.

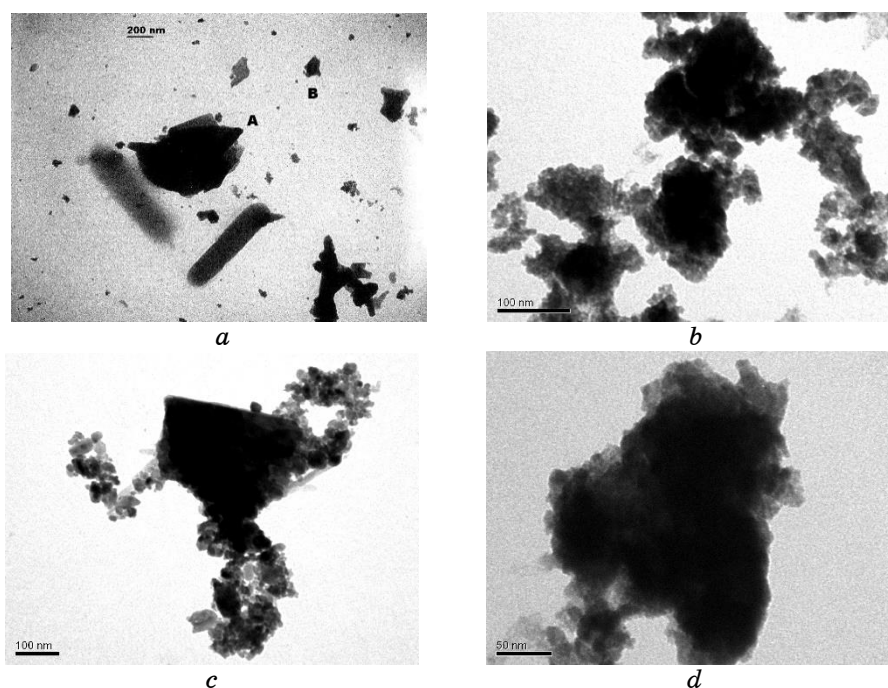
On the other hand, the formation of ZnO nanoparticles, well known photocatalyst, can lead to an increase of photocatalytic activity of the samples prepared by MChT. The study of photocatalytic activity of the samples in degradation of safranin-T dye in water solution shows (Table 5) an abrupt increase of their activity at irradiation by the visible light. The full degradation of the dye in solution was observed after 1.5 hours of irradiation.

The obtained results indicate that ZnO demonstrates a quantum-dimensional effect, and it is impossible to exclude the influence of CeO<sub>2</sub> nanoparticles as dopant of oxygen on process of dye destruction or their influence on electron-hole separation process that decreases recombination process.

**TABLE 5.** Results of porous, optical and photocatalytic studies of ZnO–CeO<sub>2</sub> systems after MChT.

Time of treatment, h	$S_{BET}$ , m <sup>2</sup> /g	$V_s \cdot 10^3$ , cm <sup>3</sup> /g	$\lambda$ , nm*	$E_g$ , eV**	$K_d \cdot 10^4$ , s <sup>-1</sup>
0	1.8	0.9	396	3.13	0.01
2	2.7	3.1	390	3.18	2.7
4	3.8	5.2	386	3,21	3.1
8	5.2	8.1	382	3,24	3.5

Note: \* $\lambda$  is the edge of the absorption band; \*\* $E_g$ —the energy of the band-gap width;  $K_d$ —constant rate of degradation dye safranin-T.


**Fig. 10.** TEM images of ZnO/CeO<sub>2</sub> samples: initial (*a*) and after MChT during 2 h, 4 h and 8 h (*b*, *c*, *d*, respectively).

#### 4. CONCLUSIONS

It was found that the mechanochemical treatment of a mixture of the ZnO and MoO<sub>3</sub> oxides permits preparation of nanodispersed phase of monoclinic  $\beta$ -ZnMoO<sub>4</sub> modification in the nanorods' form. In the case of Ce–Mo–O-system mechanochemical treatment, the formation of nanosize composites with a core–shell structure, which

contain an amorphous molybdenum oxide layer (5–15 nm) on a nucleus of nanocrystalline (25–35 nm) cerium oxide, was established. Treatment of ZnO–CeO<sub>2</sub> oxides' mixture leads to formation of nanoparticles of oxides with strong contact between them.

It was established that mechanochemically treated samples containing molybdenum ions (Zn–Mo–O, Ce–Mo–O) demonstrate high activity and selectivity at low reaction temperature in process of ethanol oxidation to acetaldehyde. The obtained results show that this process, in the presence of prepared catalysts, can be an alternative of known Wacker process of acetaldehyde fabrication. On the other hand, the samples of ZnO–CeO<sub>2</sub> composition, due to formation of nanoparticles of ZnO and possibility to promote the oxygen transport and electron–hole separation, showed a sharp increase the photocatalytic activity in process of dye degradation in water solution at visible-light irradiation.

Thus, the presented results demonstrate a significant prospect of applying the method of mechanochemistry, in its various aspects, for the synthesis of various catalytic compositions and their use in catalytic processes.

## ACKNOWLEDGMENTS

This work was supported financially by the N.A.S.U. Program of Fundamental Research 'New Functional Substances and Materials of Chemical Production' (project 13/19-21).

## REFERENCES

1. C. Suryanarayana, *Mechanochemical Alloying and Milling* (Marcel–New York: Dekker: 2004).
2. V. V. Boldyrev, *Thermochimica Acta*, **110**: 303 (1987); [https://doi.org/10.1016/0040-6031\(87\)88239-4](https://doi.org/10.1016/0040-6031(87)88239-4)
3. P. Balaz, *Extractive Metallurgy of Activated Minerals* (Amsterdam: Elsevier Science B.V.: 2000).
4. E. Avvakumov, M. Senna, and N. Kosova, *Soft Mechanochemical Synthesis: a Basis for New Chemical Technologies* (Boston: Kluwer Academic Publishers: 2002).
5. V. Zazhigalov and K. Wieczorek-Ciurowa, *Mechanochemiczna Aktywacja Katalizatorów Wanadowych* (Krakow, Polska: Wyd. Polytechn. Krakowska: 2014) (in Polish).
6. V. Molchanov and R. Buyanov, *Russian Chemical Reviews*, **69**, Iss. 5: 435 (2000); <https://doi.org/10.1070/RC2000v069n05ABEH000555>
7. S. A. Mitchenko, *Theor. Exp. Chem.*, **43**: 211 (2007); <https://doi.org/10.1007/s11237-007-0025-z>
8. P. Butyagin, *Uspekhi Khimii*, **63**: 1031 (1994) (in Russian).
9. V. Boldyrev, *Treatise on Materials Science & Technology* (Ed. Herbert

- Herman) (Elsevier: 1983), vol. 19, pt. B, p. 185;  
<https://doi.org/10.1016/B978-0-12-341842-5.50008-1>
10. E. Avvakumov, *Mechanical Methods for Activation of Chemical Processes* (Novosibirsk: Nauka: 1986) (in Russian).
  11. V. Zyryanov, *Russian Chemical Reviews*, **77**, Iss. 2: 105 (2008);  
<https://doi.org/10.1070/RC2008v077n02ABEH003709>
  12. V. Molchanov and R. Buyanov, *Kinetic and Catalysis*, **42**: 366 (2001);  
<https://doi.org/10.1023/A:1010465315877>
  13. V. Dzisko, A. Karnaukhov, and D. Tarasova, *Physicochemical Basis for the Synthesis of Oxide Catalysts* (Novosibirsk: Nauka: 1978) (in Russian).
  14. V. Dzisko, *Bases of Preparation Methods of Catalyst* (Novosibirsk: Nauka: 1983) (in Russian).
  15. J. Huang, X. Wang, S. Li, and Y. Wang, *Applied Surface Science*, **257**: 116 (2010); <https://doi.org/10.1016/j.apsusc.2010.06.046>
  16. Y. Hong, D. Chen, Z. Zhan, X. Chen, P. Lv, F. Yan, F. Huang, and J. Liang, *Journal of Alloys and Compounds*, **482**: 49 (2009);  
<https://doi.org/10.1016/j.jallcom.2009.04.045>
  17. N. Sotani, T. Suzuki, K. Nakamura, and K. Eda, *Journal of Materials Science*, **36**: 703 (2001); <https://doi.org/10.1023/A:1004893025739>
  18. Y. Keereeta, T. Thongtem, and S. Thongtem, *Superlattices and Microstructures*, **69**: 253 (2004); <https://doi.org/10.1016/j.spmi.2014.02.011>
  19. N. Enjamuri, S. Hassan, A. Auroux, J. Pandey, and B. Chowdhury, *Applied Catalysis. A: General*, **523**: 21 (2016);  
<https://doi.org/10.1016/j.apcata.2016.05.003>
  20. C. Li, X. Zhang, W. Dong, and Y. Liu, *Materials Letters*, **80**: 145 (2012);  
<https://doi.org/10.1016/j.matlet.2012.04.105>
  21. C.-F. Tseng and W.-Y. Hsu, *Thin Solid Film*, **544**: 44 (2013);  
<https://doi.org/10.1016/j.tsf.2013.05.008>
  22. M. Mohamed and S. Katib, *Applied Catalysis. A: General*, **287**: 236(2005);  
<https://doi.org/10.1016/j.apcata.2005.04.005>
  23. Y. Peng, R. Qu, X. Zhang, and J. Li, *Chemical Communications*, **49**: 6215 (2013); <https://doi.org/10.1039/C3CC42693A>
  24. Y. Jin, N. Li, H. Liu, X. Hua, Q. Zhang, M. Chen, and F. Teng, *Dalton Transactions*, **43**: 12860 (2014); <https://doi.org/10.1039/c4dt01012d>
  25. A. Sobhani-Nasab, M. Maddahfar, and S. Hosseinpour-Mashkani, *Journal of Molecular Liquids*, **216**: 1 (2016);  
<https://doi.org/10.1016/j.molliq.2015.12.104>
  26. Y. Matsuoka, M. Niwa, and Y. Murakami, *J. Phys. Chem.*, **94**: 1477 (1990);  
<https://doi.org/10.1021/j100367a051>
  27. B. Rao, P. Sudarsanam, A. Rangaswamy, and B. Reddy, *Catalysis Letters*, **145**: 1436 (2015); <https://doi.org/10.1007/s10562-015-1545-0>
  28. O. Laguna, M. Centeno, F. Romero-Sarria, and J. Odriozola, *Catalysis Today*, **172**: 118 (2011); <https://doi.org/10.1016/j.cattod.2011.02.015>
  29. N. Enjamuri, S. Hassan, A. Auroux, J. Pandey, and B. Chowdhury, *Applied Catalysis. A: General*, **523**: 21 (2016);  
<https://doi.org/10.1016/j.apcata.2016.05.003>
  30. M. Faisal, S. Khan, M. Rahman, A. Jamal, A. Asiri, and M. Abdullah, *Chemical Engineering Journal*, **173**: 178 (2011);

- <https://doi.org/10.1016/j.cej.2011.07.067>
31. K. Kaviyarasu, X. Fuku, G. Mola, E. Manikandan, J. Kennedy, and M. Maaza, *Materials Letters*, **183**: 351 (2016); <https://doi.org/10.1016/j.matlet.2016.07.143>
  32. J. Fonseca de Lima, R. Martins, and O. Serra, *Optical Materials*, **35**: 56 (2012); <https://doi.org/10.1016/j.optmat.2012.06.016>
  33. Y. Yoon, W. Ueda, and Y. Moro-oka, *Catalysis Letters*, **35**: 57 (1995); <https://doi.org/10.1007/BF00807004>
  34. G.-R. Li, Z.-L. Wang, F.-L. Zheng, and Y.-N. Ou, *J. Mater. Chem.*, **21**: 4217 (2011); <https://doi.org/10.1039/C0JM03500A>
  35. K. Nakamura, K. Eda, S. Hasegawa, and N. Sotani, *Applied Catalysis. A: General*, **178**: 167 (1999); [https://doi.org/10.1016/S0926-860X\(98\)00291-9](https://doi.org/10.1016/S0926-860X(98)00291-9)
  36. K. Kaviyarasu, X. Fuku, G. Mola, E. Manikandan, J. Kennedy, and M. Maaza, *Materials Letters*, **183**: 351 (2016); <https://doi.org/10.1016/j.matlet.2016.07.143>
  37. X. Fan, Z. Yang, W. Long, and B. Yang, *Electrochimica Acta*, **108**: 741 (2013); <https://doi.org/10.1016/j.electacta.2013.07.031>
  38. M. Zdujic and O. Milošević, *Materials Letters*, **13**: 125 (1999); [https://doi.org/10.1016/0167-577X\(92\)90122-Z](https://doi.org/10.1016/0167-577X(92)90122-Z)
  39. M. Thakare, C. Dighavkar, and J. Aher, *IJSEAS*, **2**: 137 (2016).
  40. H. Castricum, H. Bakker, and E. Poels, *Materials Science and Engineering*, **304–306**: 418 (2001); [https://doi.org/10.1016/S0921-5093\(00\)01485-4](https://doi.org/10.1016/S0921-5093(00)01485-4)
  41. Z. Marinković, L. Mančić, P. Vulić, and O. Milošević, *Journal of the European Ceramic Society*, **25**: 2081 (2005); <https://doi.org/10.1016/j.jeurceramsoc.2005.03.085>
  42. Z. Kesic, I. Lukic, M. Zdujic, H. Liu, and D. Scala, *Procedia Engineering*, **42**: 1278 (2012); <https://doi.org/10.1016/j.proeng.2012.07.509>
  43. O. Torabi, S. Naghibi, M.-H. Golabgir, and A. Jamshidi, *JCCS*, **63**: 379 (2016); <https://doi.org/10.1002/jccs.201500479>
  44. A. Firsova, O. Morozova, A. Leonov, and A. Streletskii, *Kinetic and Catalysis*, **55**: 777 (2014); <https://doi.org/10.1134/S0023158414060068>
  45. K. Milenova, K. Zaharieva, Z. Cherkezova-Zheleva, B. Kunev, A. Eliyas, V. Blaskov, I. Stambolova, and I. Mitov, *Materials, Methods & Technologies*, **8**: 241 (2014); <https://doi.org/10.1080/09593330.2011.572919>
  46. L. Morozova, A. Lapshin, T. Panova, and V. Glushkova, *Inorganic Materials*, **38**: 153 (2002); <https://doi.org/10.1023/A:1014017211450>
  47. G. Mestl, B. Herzog, R. Schlögl, and H. Knözinger, *Langmuir*, **11**: 3027 (1995); <https://doi.org/10.1021/la00008a030>
  48. S. V. Khalameida, *Mekhanokhimichna Modyfikatsia i Syntez V i Mo Vmisnykh Katalizatoriv dlya Okysnennya Nyz'kykh Vuglevodniv* [Mechanochemical Modification and Synthesis of Catalysts Containing V and Mo for Oxidation Reaction of Lower Hydrocarbons] (Thesis of Dissert. for Dr. Phys.-Chem. Sci.) (Kyiv: L. V. Pisarzhevskii Institute of Physical Chemistry, N.A.S.U.: 2000) (in Ukrainian).
  49. V. Poluboyarov, Z. Korotaeva, and O. Andryushkova, *Inorganic Materials*, **37**: 469 (2001); <https://doi.org/10.1023/A:1017585018929>
  50. N. S. Litvin, *Mekhanokhimiya Skladnykh Oksydneykh System na Osnovi Molibdena i Vanadiyu* [Mechanochemistry of Complex Oxide Systems Based on

- Molybdenum and Vanadium] (Thesis of Dissert. for Dr. Phys.-Chem. Sci.) (Kyiv: L. V. Pisarzhevskii Institute of Physical Chemistry, N.A.S.U.: 2011) (in Ukrainian).
51. K. Wieczorek-Ciurowa, N. Litvin, and V. Zazhigalov, *Przemysl Chemiczny*, **90**: 1404 (2011).
  52. V. A. Poluboyarov, *Vliyanie Mekhanicheskikh Ehffektov na Oksidnyye Sistemy Redkostnykh Metallov* [The Influence of Mechanical Effects on the Oxide Systems of Rare Metals] (Thesis of Dissert. for Dr. Phys. Chem. Sci.) (Novosibirsk: Institute of Solid State Chemistry and Mechanochemistry of the Siberian Branch of the Academy of Science: 2004) (in Russian).
  53. V. Poluboyarov, N. Chumachenko, and E. Avvakumov, *JSBAS*, **6**: 130 (1989).
  54. O. V. Andrushkova, *Issledovaniya Protsessov, Proiskhodyashchikh pri Mekhanokhimicheskoy Aktivatsii Oksidov Metallov II–VIII Grupp* [The Study of the Processes Occurring at the Mechanochemical Activation of Metal Oxides of Groups II–VIII] (Thesis of Dissert. for Dr. Phys. Chem. Sci.) (Novosibirsk: Institute of Solid State Chemistry and Mechanochemistry of the Siberian Branch of the Academy of Science: 1993) (in Russian).
  55. V. Zazhigalov, L. Bogutskaya, L. Lyashenko, and S. Khalameida, *Mechanochemical Processes* (Odesa: Votum: 1997).
  56. V. Poluboyarov, I. Pauli, S. Kiselevich, and Z. Korotaeva, *Mechanochemical Processes* (Odesa: Votum: 1997), p. 15.
  57. V. Poluboyarov, S. Kiselevich, O. Kirichenko, I. Pauli, Z. Korotaeva, S. Dektyarov, and A. Ancharov, *Inorganic Materials*, **34**: 1365 (1998).
  58. V. Zazhigalov, K. Wieczorek-Ciurowa, I. Bacherikova, and L. Depero, *2<sup>nd</sup> International Congress on Green Process Engineering - GPE 2009 (14–17 June 2009, Venice, Italy)*, p. 103.
  59. V. Zazhigalov, I. Bacherikova, S. Khalameida, N. Litvin, K. Wieczorek-Ciurowa, L. Depero, and A. Kowal, *6<sup>th</sup> World Congr. Oxid. Catal.* (Lille: 2009), p. 54.
  60. V. Zazhigalov, *Theoretical and Experimental Chemistry*, **49**: 178 (2013); <https://doi.org/10.1007/s11237-013-9312-z>
  61. J. Tatibouet, Ch. Phichitkul, and J. Germain, *Journal of Catalysis*, **99**: 231 (1986); [https://doi.org/10.1016/0021-9517\(86\)90216-2](https://doi.org/10.1016/0021-9517(86)90216-2)
  62. J. Vedrine, G. Coudurier, M. Forissier, and J. Volta, *Catalysis Today*, **1**: 261 (1987); [https://doi.org/10.1016/0920-5861\(87\)80011-1](https://doi.org/10.1016/0920-5861(87)80011-1)
  63. A. Baiker, P. Dollenmeier, and A. Reller, *Journal of Catalysis*, **103**: 394 (1987); [https://doi.org/10.1016/0021-9517\(87\)90130-8](https://doi.org/10.1016/0021-9517(87)90130-8)
  64. W. Farneth, E. McCarron, A. Sleight, and R. Staley, *Langmuir*, **3**: 217 (1987); <https://doi.org/10.1021/la00074a013>
  65. G. Mestl, N. Verbruggen, and H. Knözinger, *Langmuir*, **11**: 3035 (1995); <https://doi.org/10.1021/la00008a031>.
  66. V. Zazhigalov, L. Bogutskaya, L. Lyashenko, and S. Khalameida, *TOCAT-3–Adv. Catal. Sci. Techn.* (Tokyo: 1998), p. 348.
  67. L. Bogutskaya, S. Khalameida, V. Zazhigalov, A. Kharlamov, L. Lyashenko, and O. Byl', *Theoretical and Experimental Chemistry*, **35**: 242 (1999); <https://doi.org/10.1007/BF02511524>
  68. V. A. Zazhigalov, S. V. Khalameida, and L. V. Bogutskaya, *DGMK* (Erlan-

- gen: 1999), p. 215.
69. V. Zazhigalov, A. Kharlamov, S. Khalameida, I. Bacherikova, and L. Depero, *Dutch–Ukrainian Intern. Colloq. Catal.* (Kiev: 2000), p. 46.
  70. B. Krebs, *Acta Cryst.*, **28**: 2222 (1972); <https://doi.org/10.1107/S0567740872005849>
  71. G. Centi, F. Cavani, and F. Trifiro, *Selective Oxidation by Heterogeneous Catalysis* (New York: Kluwer: 2001), p. 505.
  72. E. Smolentseva, A. Simakov, S. Beloshapkin, M. Estrada, E. Vargas, V. Sobolev, R. Kenzhin, and S. Fuentes, *Applied Catalysis. B: Environmental*, **115–116**: 117 (2012); <https://doi.org/10.1016/j.apcatb.2011.12.010>
  73. Y. Dimitriev, R. Iordanova, and M. Markova-Velichkova, *Journal of the University of Chemical Technology and Metallurgy*, **46**: 249 (2011).
  74. V. Zazhigalov, E. Sachuk, N. Kopachevskaya, I. Bacherikova, K. Wieczorek-Ciurowa, and S. Shcherbakov, *Theoretical and Experimental Chemistry*, **52**: 97 (2016); <https://doi.org/10.1007/s11237-016-9456-8>
  75. O. Sachuk, V. Zazhigalov, L. Kuznetsova, and M. Tsyba, *CICS*, **7**: 309 (2016) (in Ukrainian); <https://doi.org/10.15407/hftp07.03.309>
  76. L. Damonte, M. Hernández, and B. Mari, *Journal of Alloys and Compounds*, **434–435**: 813 (2007); <https://doi.org/10.1016/j.jallcom.2006.08.202>
  77. A. M. Glushenkov, H. Z. Zhang, and Y. Chen, *Materials Letters*, **62**: 715 (2008); <https://doi.org/10.1016/j.matlet.2008.06.002>
  78. V. Boldyrev, *Process Metallurgy*, **10**: 1 (2000); [https://doi.org/10.1016/S1572-4409\(00\)80002-4](https://doi.org/10.1016/S1572-4409(00)80002-4)
  79. Y. Liang, P. Liu, H. Li, and G. Yang, *Cryst. Growth Des.*, **12**: 4487 (2012); <https://doi.org/10.1021/cg3006629>
  80. J. Rou, S.-M. Koo, J.-W. Yoon, C. Lim, and K. Shim, *Materials Letters*, **60**: 1702 (2006); <https://doi.org/10.1016/j.matlet.2005.12.018>
  81. M. Markova-Velichkova, R. Iordanova, and Y. Dimitriev, *Physica Status Solidi C*, **8**: 3159 (2011); <https://doi.org/10.1002/pssc.201000752>
  82. D. Agarwal, D. Avasthi, S. Varma, F. Kremer, M. Ridgway, and D. Kabiraj, *Journal of Applied Physics*, **115**: 163506 (2014); <https://doi.org/10.1063/1.4872259>
  83. G. Boreskov, *Heterogennyy Cataliz* (Moscow: Nauka: 1986) (in Russian).
  84. V. Zazhigalov, A. Kharlamov, L. Depero, A. Marino, I. Bacherikova, S. Khalameida, and E. Stokch, *Theoretical and Experimental Chemistry*, **36**: 98 (2000); <https://doi.org/10.1007/BF02529026>
  85. N. Li, Y. Li, and W. Li, *J. Phys. Chem. C*, **120**: 3341 (2016); <https://doi.org/10.1021/acs.jpcc.5b10752>.
  86. V. Zazhigalov, K. Wieczorek-Ciurowa, O. Sachuk, E. Diyuk, and I. Bacherikova, *Theoretical and Experimental Chemistry*, **54**: 225 (2018); <https://doi.org/10.1007/s11237-018-9567-5>
  87. S. Warule, N. Chaudhari, B. Kale, K. Patil, P. Koinkar, M. More, and R. Murakami, *J. Mater. Chem.*, **22**: 8887 (2012); <https://doi.org/10.1039/C2JM30226H>